*fractal and fractional*

MDPI

*Article*

# Response of Green Bonds and Sustainable Equity Markets to Crisis Regimes: A Dynamic Multifractal Efficiency Assessment

**Fernando Henrique Antunes de Araujo [1,*], Milena Kojić [2,3] and Petar Mitić [3]**

[1] Campus Patos, Federal Institute of Education, Science and Technology of Paraiba (IFPB), Rodovia PB-110, s/n, Alto da Tubiba, Patos 58700-030, Brazil
[2] Department of Mathematics and Statistics, College of Arts, Sciences and Education, Florida International University, 11101 SW 13th St, Miami, FL 33174, USA; mkojic@fiu.edu
[3] Institute of Economic Sciences, Zmaj Jovina 12, 11000 Belgrade, Serbia; petar.mitic@ien.bg.ac.rs
* Correspondence: fernando.araujo@ifpb.edu.br

**Abstract**

This article examines whether the informational efficiency of green bonds and sustainability-oriented equity indices changes across crisis regimes. Methods: We analyze the S&P Green Bond Index and eight S&P sustainable equity indices from 16 February 2016 to 10 November 2025 using static and rolling-window multifractal detrended fluctuation analysis. Rolling inefficiency, defined as the absolute deviation of the singularity-spectrum peak from 0.5, is then modelled with crisis-regime indicators, asset effects, dependence-robust inference, and window-level risk controls. Results: The S&P Green Bond Index remains among the most efficient and least volatile assets in the sample. Crisis-labelled windows display higher multifractal inefficiency than the pre-COVID benchmark, although the robustness checks show that part of the raw effect is transmitted through volatility and tail-risk conditions. Conclusions: Sustainable-finance efficiency is nonlinear and regime dependent, and the evidence is interpreted as a conditional association rather than causal identification. Green bonds are comparatively resilient, but not informationally invariant during systemic, geopolitical, and policy-driven stress.

**Keywords:** green bonds; sustainable equity indices; market efficiency; multifractal detrended fluctuation analysis; crisis regimes; robustness checks

## 1. Introduction

Green bonds have evolved from a specialized financing instrument into a central building block of the broader sustainable-finance architecture. Initially designed to direct capital toward environmentally beneficial projects, they are now increasingly assessed not only for their environmental purpose but also for the quality of their risk–return properties in diversified portfolios [1–4].

Most of the empirical literature evaluates green bonds through hedging, diversification, and safe-haven frameworks. That line of research documents episodes in which green bonds decouple from risky assets, but it also shows that those benefits weaken when stress becomes systemic or when downside dependence intensifies [5–10]. While such evidence is highly informative, it does not fully resolve a deeper question: do green bonds and sustainable equity markets themselves remain informationally efficient when crises reshape the nonlinear dynamics of returns?

From a theoretical standpoint, this question sits at the intersection of three views of market behaviour. The classical Efficient Market Hypothesis treats prices as information-efficient

Check for updates

Academic Editors: Bruce Henry and Pedro Chamorro-Posada

Received: 28 April 2026
Revised: 24 May 2026
Accepted: 3 June 2026
Published: 8 June 2026

signals [11], but the Grossman–Stiglitz paradox shows that perfectly revealing prices are difficult to reconcile with costly information acquisition [12]. The Adaptive Markets Hypothesis then suggests that efficiency should be interpreted as an evolving outcome of competition, learning, and changing market ecology rather than as a permanent state [13].

That question is particularly relevant for sustainable assets because they are exposed to multiple and partly overlapping sources of uncertainty. Climate risk, transition policy, commodity repricing, geopolitical fragmentation, and macro-financial turbulence affect the sustainable-investment universe through different transmission channels. A market that appears stable under one type of shock may exhibit persistence, predictability, or stronger long-range dependence under another. In addition, sustainable assets are not priced solely by conventional cash-flow and discount-rate news. Investor sustainability preferences, climate-hedging demand, and segmented debt-market clienteles can alter both expected returns and liquidity conditions [14,15]. For that reason, a static efficiency test is unlikely to be sufficient.

Multifractal methods provide a natural way to address this problem. They are explicitly designed to capture scale heterogeneity, nonlinear dependence, and the asymmetric contribution of small and large fluctuations. This logic is closely related to the multifractal model of asset returns, in which heavy tails, volatility persistence, and heterogeneous local regularity arise jointly rather than as isolated anomalies [16]. In the green-finance literature, recent studies show that green bonds and related sustainable assets exhibit multifractal features, time-varying efficiency, and crisis-sensitive dynamics, especially around COVID-19 and other periods of elevated uncertainty [17–21]. In the broader market-efficiency literature, multifractal evidence is also consistent with the view that efficiency evolves through time as agents adapt to information, learning, and changes in market structure [13,22–24].

This study contributes to that literature in four ways. First, it combines the S&P Green Bond Index with eight heterogeneous sustainability-oriented equity benchmarks, thus capturing both bond and equity dimensions of sustainable investing. Second, it measures efficiency with the same MFDFA framework in both the full sample and rolling windows, ensuring consistency between long-run and local estimates. Third, it explicitly compares multiple stress regimes rather than a single crisis, distinguishing between a systemic health shock, two geopolitical conflicts, and a policy-driven trade episode. Fourth, it complements the multifractal evidence with OLS and quantile panel regressions to evaluate whether crisis effects remain significant once cross-sectional asset heterogeneity is controlled for.

The results reveal that the S&P Green Bond Index is one of the most efficient assets in the sample, ranking fourth overall, and it is by far the least volatile. Nevertheless, average rolling inefficiency rises by 133.9% during COVID-19, by 50.6% during the Russia–Ukraine period, by 91.9% during the Israel–Hamas period, and by 75.9% during the U.S. tariff episode relative to the pre-pandemic benchmark. These findings indicate resilience, but not invariance, and support a regime-dependent interpretation of informational efficiency in sustainable finance.

## 2. Data and Crisis Segmentation

The empirical sample contains nine daily S&P indices. The fixed-income leg is represented by the S&P Green Bond Index, while the equity leg comprises sustainability-oriented benchmarks covering natural resources, carbon efficiency, environmental and social responsibility, clean energy transition, scored-and-screened equities, infrastructure, sustainability screening, and water. The observation window runs from 16 February 2016 to 10 November 2025, which is the longest period over which the full cross-section can be aligned without synthetic interpolation.

This cross-section is theoretically attractive because it combines instruments exposed to different pricing mechanisms inside sustainable finance. Green bonds are shaped by a labelled use-of-proceeds design, investor clienteles, and debt-market liquidity conditions, whereas the equity indices embed sector composition, transition exposure, and ESG screening rules [3,14,15]. Comparing them inside a common multifractal framework therefore helps distinguish general sustainable-finance stress from asset-class-specific nonlinearities (Table 1).

**Table 1.** Analyzed indices, empirical role, and data source.

| Code | Index | Index Family | Role in the Empirical Design | Measurement/Source |
|---|---|---|---|---|
| GNR | S&P Global Natural Resources Index | Sustainability-oriented equity benchmark | Input index-level series; cross-sectional unit in the panel stage | S&P index level collected from the secondary dataset supplied to the authors |
| CEI | S&P 500 Carbon Efficient Index (USD) | Sustainability-oriented equity benchmark | Input index-level series; cross-sectional unit in the panel stage | S&P index level collected from the secondary dataset supplied to the authors |
| ESR | S&P 500 Environmental & Socially Responsible Index | Sustainability-oriented equity benchmark | Input index-level series; cross-sectional unit in the panel stage | S&P index level collected from the secondary dataset supplied to the authors |
| CET | S&P Global Clean Energy Transition Index (USD) | Sustainability-oriented equity benchmark | Input index-level series; cross-sectional unit in the panel stage | S&P index level collected from the secondary dataset supplied to the authors |
| SSC | S&P 500 Scored & Screened Index (USD) | Sustainability-oriented equity benchmark | Input index-level series; cross-sectional unit in the panel stage | S&P index level collected from the secondary dataset supplied to the authors |
| GII | S&P Global Infrastructure Index | Sustainability-oriented equity benchmark | Input index-level series; cross-sectional unit in the panel stage | S&P index level collected from the secondary dataset supplied to the authors |
| SUS | S&P 500 Sustainability Screened Index (USD) | Sustainability-oriented equity benchmark | Input index-level series; cross-sectional unit in the panel stage | S&P index level collected from the secondary dataset supplied to the authors |
| WAT | S&P Global Water Index | Sustainability-oriented equity benchmark | Input index-level series; cross-sectional unit in the panel stage | S&P index level collected from the secondary dataset supplied to the authors |
| GBD | S&P Green Bond Index | Green bond fixed-income benchmark | Input index-level series; cross-sectional unit in the panel stage | S&P index level collected from the secondary dataset supplied to the authors |

The raw indices are not used as dependent or independent variables directly. They are input series from which daily returns and rolling MFDFA inefficiency are estimated. In the regression stage, rolling inefficiency is the dependent variable, crisis-regime indicators are the main predictors, and asset fixed effects plus window-level risk controls are used to absorb cross-sectional and distributional heterogeneity.

These indices differ not only in sustainability orientation but also in construction methodology, and this distinction affects interpretation. Several equity indices, including CEI, ESR, SSC, and SUS, are derived from the S&P 500 universe through carbon-efficiency tilts, ESG screening, or scoring overlays. Their return dynamics are therefore likely to reflect broad U.S. large-cap equity behaviour, with sustainability-related adjustments operating around that parent-index structure. By contrast, GNR, CET, GII, and WAT are global thematic indices built from narrower sector universes, including natural resources, clean energy, infrastructure, and water. Their risk profiles are more directly shaped by commodity cycles, energy policy, infrastructure regulation, input-cost dynamics, and sector-specific repricing. The green bond benchmark, GBD, is a fixed-income index and therefore follows a different return-generating process from the equity benchmarks. Consequently, observed differences in multifractal properties may reflect sectoral concentration, regional composition, and asset-class mechanics as well as sustainability labelling. A cleaner separation of sustainability-specific effects from these structural differences would require matched conventional benchmarks for each index, which are not included in the present dataset.

All indices were collected from the secondary S&P index-level dataset supplied to the authors; the indices were not constructed by the authors. The empirical contribution lies in transforming these observed index levels into log returns, estimating multifractal efficiency metrics, and testing whether crisis-regime indicators explain the resulting rolling inefficiency. Because the source file does not separately flag each series as a total-return or price-return index, the manuscript refers to observed index levels, defines returns strictly as log differences in those observed levels, and avoids interpreting dividend-reinvestment or coupon-reinvestment effects as independent empirical findings.

This qualification is important because total-return indices, which reinvest coupon or dividend income, may contain a smoother income-related component than price-return indices. If the green bond benchmark is reported on a total-return basis while some equity benchmarks are reported on a price-return basis, part of the observed difference in scaling properties could mechanically reflect reinvested income rather than differences in informational efficiency alone. The cross-asset results should therefore be interpreted as evidence based on the observed index-level series available to the authors, while future work should verify and harmonize return definitions before attributing cross-sectional differences to market microstructure, investor behaviour, or sustainability-related pricing channels.

Returns are defined as logarithmic first differences in daily index levels. This transformation is standard in financial applications because it stabilizes scale, facilitates interpretation in approximate percentage terms, and provides a stationary input for multifractal analysis.

$$r_t = ln(P_t) - ln(P_{t-1}) \tag{1}$$

Table 2 already indicates substantial heterogeneity. The green bond benchmark records the lowest annualized volatility in the sample (0.0598), whereas the clean energy transition index is the most volatile. Among the equity series, sustainability-screened, scored-and-screened, and environmental socially responsible indices display the highest annualized mean returns. The starting point of the multifractal analysis is therefore a cross-section that differs not only in sectoral content but also in conventional risk–return terms.

**Table 2.** Descriptive statistics of daily log returns.

| Code | Index | Obs. | Annualized Mean | Annualized Volatility | Daily Min. | Daily Max. |
|---|---|---|---|---|---|---|
| GNR | S&P Global Natural Resources Index | 2616 | 0.0521 | 0.1944 | −0.1291 | 0.1169 |
| CEI | S&P 500 Carbon Efficient Index (USD) | 2524 | 0.1137 | 0.1819 | −0.1307 | 0.0918 |
| ESR | S&P 500 Environmental & Socially Responsible Index | 2524 | 0.1225 | 0.1848 | −0.1255 | 0.0933 |
| CET | S&P Global Clean Energy Transition Index (USD) | 2609 | 0.0523 | 0.2392 | −0.1250 | 0.1103 |
| SSC | S&P 500 Scored & Screened Index (USD) | 2524 | 0.1232 | 0.1832 | −0.1277 | 0.0915 |
| GII | S&P Global Infrastructure Index | 2605 | 0.0424 | 0.1509 | −0.1432 | 0.0999 |
| SUS | S&P 500 Sustainability Screened Index (USD) | 2524 | 0.1244 | 0.1872 | −0.1297 | 0.0943 |
| WAT | S&P Global Water Index | 2614 | 0.0804 | 0.1573 | −0.1114 | 0.0753 |
| GBD | S&P Green Bond Index | 2614 | 0.0124 | 0.0598 | −0.0241 | 0.0227 |

Annualized mean equals the daily mean multiplied by 252. Annualized volatility equals the daily standard deviation multiplied by the square root of 252.

To study regime dependence (Table 3), the sample is partitioned into five crisis states beyond the full sample: a pre-COVID benchmark, the COVID-19 crisis, the Russia–Ukraine war, the Israel–Hamas conflict, and the U.S. tariff episode associated with the second Trump administration. The segmentation is motivated by the fact that these episodes differ materially in origin and transmission mechanism. COVID-19 was a systemic shock that compressed global market conditions; the later episodes were more explicitly geopolitical or policy-driven and therefore more likely to generate asset-specific responses. This distinction matters theoretically because fractal and adaptive views of financial markets imply that stress episodes need not affect the full spectrum of investment horizons in the same way [24,25].

The crisis regimes are therefore used as temporal proxies for information environments rather than as traded assets or macroeconomic factors. Operationally, the proxies are date-based dummy variables: COVID-19, Russia–Ukraine, Israel–Hamas, and U.S. tariffs each equal one when the ending date of a rolling window falls inside the corresponding period and zero otherwise. The pre-COVID regime is the omitted benchmark. The dependent variable is the MFDFA-based rolling inefficiency score, so the crisis dummies measure whether the local scaling structure of returns differs from the pre-COVID benchmark (Figures 1 and 2).

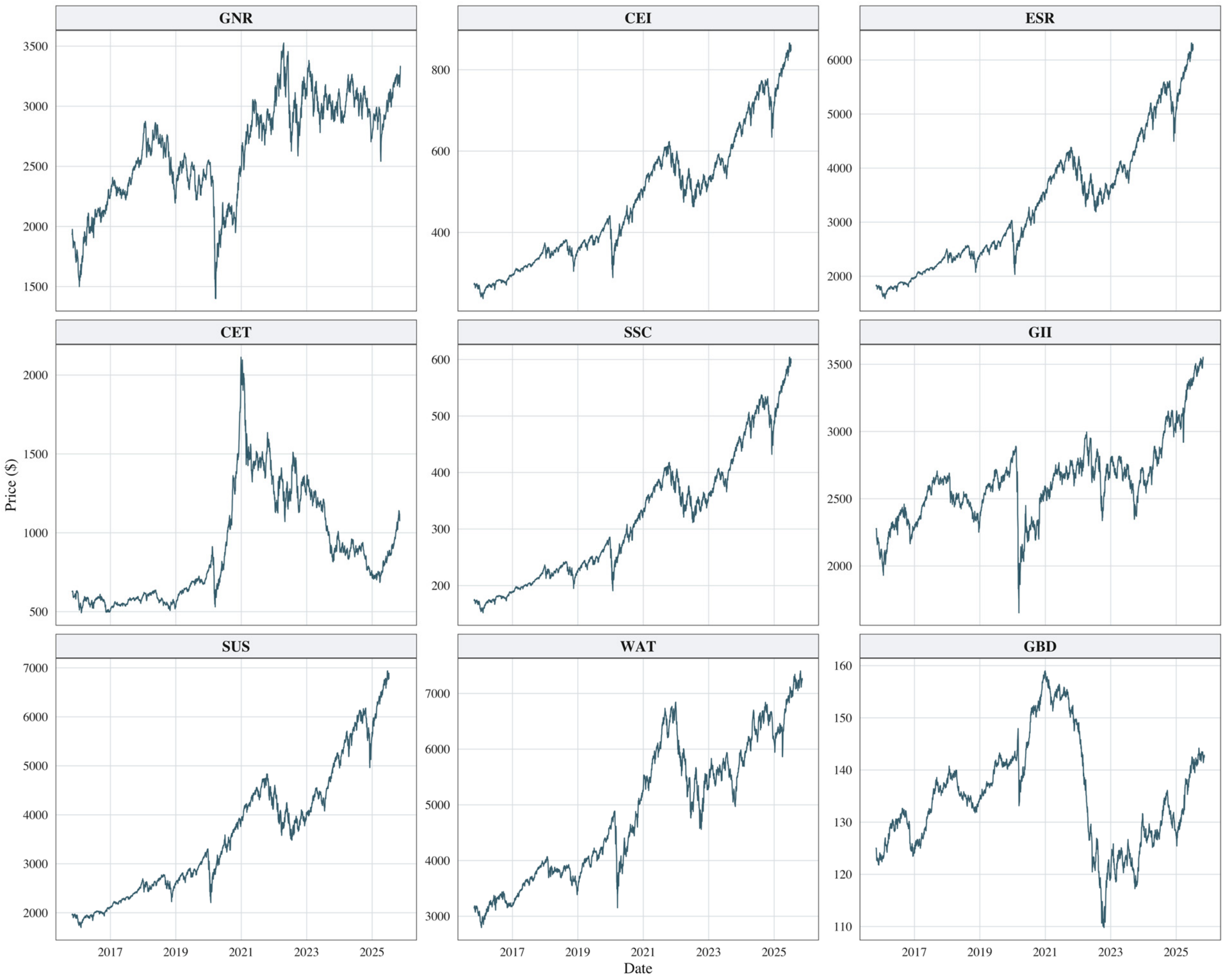


**Figure 1.** Original index levels for the nine analyzed assets over the common sample.

**Table 3.** Crisis-regime proxies used in the rolling-window analysis.

| Period | Start Date | End Date | Description |
|---|---|---|---|
| Full sample | 16 February 2016 | 10 November 2025 | Entire dataset used for the static MFDFA estimates and as the source universe for the rolling analysis. |
| Before COVID-19 period | 16 February 2016 | 31 December 2019 | Pre-pandemic benchmark period used as the reference state in the dynamic analysis. |
| COVID-19 crisis period | 1 January 2020 | 30 April 2021 | Window associated with the outbreak, diffusion, and acute financial turbulence of the pandemic. |
| Russia–Ukraine war period | 24 February 2022 | 31 May 2023 | Geopolitical shock linked to the invasion of Ukraine and the repricing of energy and commodity risks. |
| Israel–Hamas conflict period | 7 October 2023 | 29 February 2024 | Conflict period marked by renewed geopolitical uncertainty and regional spillovers. |
| U.S. tariffs—Trump's second term | 20 January 2025 | 10 November 2025 | Policy-driven period associated with renewed tariff measures and trade-policy uncertainty. |

The full sample is reported for completeness. In the rolling analysis, each 500-trading-day window is assigned to the regime in which its ending date falls. This rule is a transparent classification device for overlapping windows, not a claim that the full information content of each window originates inside only one regime. The extent of cross-regime contamination can be substantial near regime boundaries. A 500-trading-day window ending shortly after the start of a crisis regime may contain only a small fraction of observations from the labelled period, with the remaining observations drawn from the preceding state. The share of labelled-regime observations increases for windows ending later in each episode, but even mid-regime windows may still contain information from earlier market conditions. The crisis coefficients should therefore be interpreted as capturing gradual changes in rolling scaling properties around crisis-labelled periods, rather than as clean within-regime estimates.

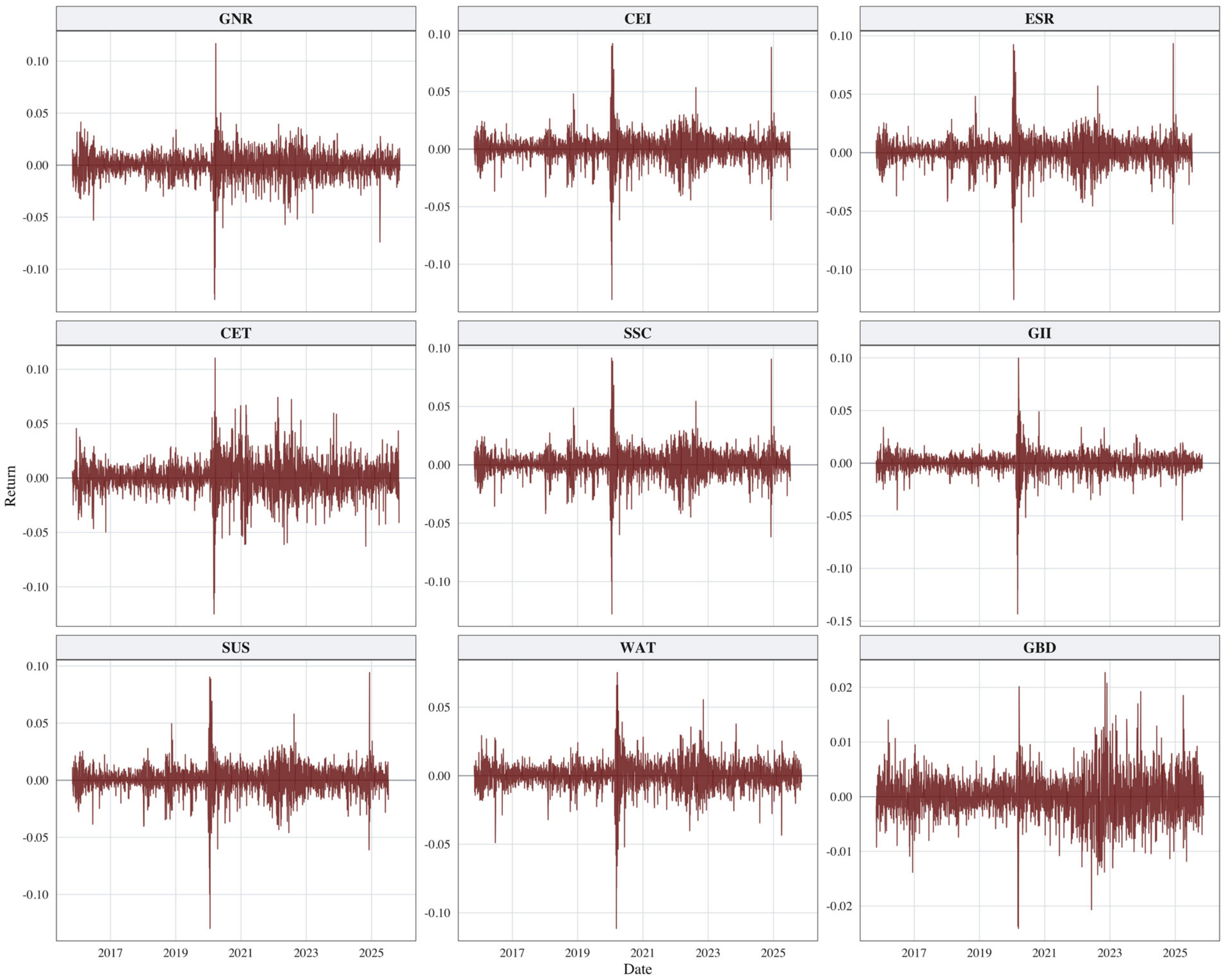


**Figure 2.** Daily log returns corresponding to the original index series.

## 3. Methodology

The methodology follows three principles. First, the paper studies informational efficiency in the time-series sense, not mean-variance portfolio efficiency. Second, the crisis variables are regime indicators used to explain rolling inefficiency, not assets whose performance is being tested against a market factor. Third, all regression evidence is interpreted as reduced-form association between regimes and multifractal inefficiency, with additional checks for overlapping-window dependence and distributional conditions.

The empirical strategy follows multifractal detrended fluctuation analysis (MFDFA), originally proposed by [26]. MFDFA is appropriate for financial returns because it measures scaling behaviour across multiple time horizons while remaining robust to nonstationary level effects. In practical terms, it detects whether small and large fluctuations scale differently and whether dependence patterns remain stable or vary across the distribution of shocks. This is precisely the type of structure that multifractal asset-pricing models attempt to formalize when they relate heavy tails, long-memory in volatility, and heterogeneous local regularity to a common scaling mechanism [16].

### *3.1. Static Multifractal Detrended Fluctuation Analysis*

Let $r_t$ denote the return series of length N. The first step is to construct the profile of the demeaned series, that is, the cumulative sum of deviations from the sample mean. This transformation converts the original return sequence into an integrated process whose local trends can be filtered out scale by scale.

$$Y(i) = \Sigma_{k=1}^{i} \left[ r_k - r^{-} \right] \tag{2}$$

For each scale s, the profile is partitioned into $N_s$ = floor (N/s) non-overlapping segments. Because N is not necessarily a multiple of s, the segmentation is performed twice: once from the beginning of the profile and once from the end. This produces $2N_s$ segments and prevents the observations in the tail of the series from being discarded at a given scale.

Within every segment, a local deterministic trend is estimated by least squares and then removed. In the empirical implementation used here, the detrending polynomial is first order, which means that the method filters local linear drift while preserving higher-order fluctuations. The detrended variance for segment ν at scale s is then computed as follows:

$$F^2(\nu, s) \;=\; (1/s)\; \Sigma_{i=1}^{s} \left[ Y((\nu-1)s \;+\; i) \;-\; y_{\nu}(i) \right]^2 \tag{3}$$

The next step aggregates these detrended variances through the q-order fluctuation function $F_q(s)$. Positive q values increase the weight of large fluctuations, whereas negative q values give relatively greater weight to small fluctuations. Consequently, the behaviour of $F_q(s)$ across q reveals whether the series has a single scaling law or whether different parts of the fluctuation distribution are governed by different effective exponents.

$$F_q(s) = \{ (1/2N_{\,s})\; \Sigma_{\nu=1} 2N_s\; [F^{\,2}(\nu, s)]^{q/2} \}^{1/q} \tag{4}$$

The general expression above is undefined at q = 0. To avoid that singularity, the q = 0 case is obtained through the logarithmic mean, which corresponds to the continuous limit of $F_q(s)$.

$$F_0(s) = exp\{ (1/4N_{\,s})\; \Sigma_{\nu=1} 2N_s\; ln[F^{\,2}(\nu, s)] \} \tag{5}$$

If the process obeys a scale-invariant law, the fluctuation function grows as a power of s. The slope of the log–log relationship is the generalized Hurst exponent h(q). A monofractal process would yield a constant h(q), whereas a multifractal process exhibits an h(q) that changes with q, meaning that different parts of the return distribution obey different scaling regimes.

$$F_q(s) \sim s^{h(q)} \tag{6}$$

The generalized Hurst exponent is then translated into the mass exponent and, through a Legendre transform, into the singularity spectrum. The mass exponent summarizes how statistical moments scale with q, while the singularity spectrum describes the distribution of local Hölder exponents in the series. These quantities are central because they transform raw scaling information into interpretable measures of persistence, heterogeneity, and complexity.

$$\tau(q) = qh(q) - 1 \tag{7}$$

$$\alpha(q) = \partial\tau(q)/\partial q \tag{8}$$

$$f(\alpha) = q\alpha - \tau(q) \tag{9}$$

Three spectrum-based statistics are used in the article. The first is the peak of the spectrum, $\alpha_0$, which is interpreted as the central persistence parameter. Values close to 0.5 indicate approximately random dynamics. Values above 0.5 suggest persistence, meaning that returns tend to continue in the same direction, whereas values below 0.5 suggest anti-persistence and mean-reverting behaviour. The second is the spectrum width, which measures the degree of multifractality. The third is the asymmetry of the spectrum, which indicates whether multifractality is more strongly associated with small or large fluctuations.

$$Inefficiency = |\alpha_0 - 0.5| \tag{10}$$

The primary inefficiency indicator is the absolute deviation of $\alpha_0$ from 0.5. This choice treats $\alpha_0$ as the main operational indicator of time-series persistence, not as a sufficient statistic for every dimension of market efficiency. The rationale is that the peak of the singularity spectrum gives a compact estimate of the dominant local scaling exponent: values close to 0.5 are consistent with weak persistence around the random-walk benchmark, whereas values farther from 0.5 indicate stronger local persistence or anti-persistence. This operational definition is also consistent with previous dynamic multifractal studies of financial-market inefficiency that use the distance from the random-walk benchmark to quantify inefficiency; two such applications examine Chinese sectoral indices during COVID-19, and a related study analyzes USA education-group stocks before, during, and after COVID-19 [27–29]. The article does not discard the rest of the spectrum. Spectrum width and asymmetry are reported as complementary diagnostics because they capture heterogeneity between small and large fluctuations, while h(2), entropy-based indicators, and composite metrics would answer related but not identical measurement questions. Entropy-based approaches provide a complementary view of efficiency during crises [30], and portfolio-efficiency tests such as the GRS framework address a distinct mean-variance question rather than the time-series predictability studied here [31].

### 3.2. Rolling-Window Implementation and Crisis Assignment

The static analysis is complemented by a rolling implementation of MFDFA. Each window contains 500 trading days, approximately two calendar years of observations, and consecutive windows are advanced by 21 trading days, approximately one trading month. This design deliberately balances two competing requirements: MFDFA needs enough observations inside each window to estimate scaling exponents over multiple scales, while the crisis analysis requires enough local estimates to observe changes across regimes.

For each rolling window, the same 22 logarithmically spaced scales are used, q varies from −10 to 10 in steps of 2, and first-order detrending removes local linear drift. These parameter choices follow common MFDFA practice, but they are treated as modelling choices rather than immutable truths. They define the main empirical specification rather than a claim that every alternative detrending order, scale range, or q-grid would deliver numerically identical estimates. Full parameter-grid sensitivity, especially for higher-order detrending and narrower q ranges, remains a useful extension and is acknowledged as a limitation of the study. The overlap between windows is explicitly acknowledged: adjacent estimates share many observations, so the regression stage uses dependence-robust inference and the robustness section reports a non-overlapping-window sensitivity check.

### *3.3. Regression Framework*

To complement the descriptive rolling evidence, window-level inefficiency is regressed on crisis dummies, asset effects, and distributional controls computed inside each rolling window. The dependent variable is rolling inefficiency, defined as $|\alpha_0 - 0.5|$. The main predictors are the COVID-19, Russia–Ukraine, Israel–Hamas, and U.S. tariff regime indicators. The pre-COVID period is the omitted benchmark.

$$IE_{i,t} = \beta_0 + \beta_1\, COVID_t + \beta_2\, RU_t + \beta_3\, IH_t + \beta_4\, TAR_t + \gamma_i + \varepsilon_{i,t} \tag{11}$$

where $\mathrm{IE_{it}}$ is rolling inefficiency for asset i in window t, COVIDt, RUt, IHt, and TARt are crisis indicators, $\gamma_\mathrm{i}$ captures asset fixed effects, and $\varepsilon_\mathrm{it}$ is the idiosyncratic disturbance. Because crisis effects may differ between relatively efficient and relatively inefficient states, the article also estimates quantile regressions:

$$Q_\tau(IE_{i,t} \mid X_{i,t}) = X_{i,t}{}'\beta_\tau \tag{12}$$

This second specification reveals whether crisis regimes shift the entire inefficiency distribution or primarily affect its upper tail. That distinction is economically meaningful because systemic or policy shocks may be mild in average conditions but much stronger when the market is already in a high-persistence state.

Because the rolling windows overlap heavily, conventional standard errors may overstate precision. The empirical analysis therefore reports two-way clustered standard errors by asset and rolling-window identifier for the OLS stage. This clustering structure addresses two distinct dimensions of dependence: repeated observations within the same asset and common window-level shocks across assets. It should be read as a dependence-robust correction rather than as a complete cure for the mechanical dependence created by overlapping windows. For that reason, the analysis also reports a non-overlapping-window diagnostic, which imposes a more severe reduction in overlap at the cost of much lower statistical power. The regression section further adds a controlled specification with realized volatility, downside semideviation, and the 95th percentile of absolute returns, which helps distinguish crisis-regime effects from changes in volatility, downside risk, and tail behaviour.

## 4. Empirical Results and Discussion

### *4.1. Descriptive Evidence*

The descriptive statistics already suggest that the sample is economically heterogeneous. The S&P Green Bond Index is distinctly less volatile than the sustainable equity series and displays a comparatively compressed return range. At the opposite end, the clean energy transition index exhibits the highest annualized volatility, while sustainability-screened and scored-and-screened indices produce the largest annualized mean returns. This heterogeneity matters because multifractal efficiency is not evaluated over a set of near-identical series, but over assets with different sectoral structures, risk exposures, and likely investor clienteles.

### 4.2. Full-Sample Multifractal Evidence

The full-sample evidence is presented first because it establishes the benchmark ordering of assets before the analysis moves to local and crisis-specific dynamics. Table 4 condenses the ranking and the main spectrum-based metrics, while Figure 3 illustrates the underlying multifractal objects that generate those summary measures.

**Table 4.** Full-sample multifractal metrics and efficiency ranking.

| Rank | Code | Index | $\alpha_0$ | Inefficiency | Spectrum Width | Asymmetry |
|---|---|---|---|---|---|---|
| 1 | ESR | S&P 500 Environmental & Socially Responsible Index | 0.4995 | $5 \times 10^{-4}$ | 1.3451 | 0.2131 |
| 2 | CEI | S&P 500 Carbon Efficient Index (USD) | 0.4979 | 0.0021 | 1.2741 | 0.2205 |
| 3 | SSC | S&P 500 Scored & Screened Index (USD) | 0.4963 | 0.0037 | 1.4521 | 0.197 |
| 4 | GBD | S&P Green Bond Index | 0.504 | 0.004 | 0.8381 | 0.317 |
| 5 | GII | S&P Global Infrastructure Index | 0.5077 | 0.0077 | 0.9095 | 0.315 |
| 6 | WAT | S&P Global Water Index | 0.5123 | 0.0123 | 1.2703 | 0.2498 |
| 7 | SUS | S&P 500 Sustainability Screened Index (USD) | 0.4875 | 0.0125 | 1.0716 | 0.2491 |
| 8 | GNR | S&P Global Natural Resources Index | 0.5251 | 0.0251 | 2.4058 | 0.1368 |
| 9 | CET | S&P Global Clean Energy Transition Index (USD) | 0.5358 | 0.0358 | 1.153 | 0.2239 |

Inefficiency equals $|\alpha_0 - 0.5|$. Lower values imply greater proximity to the efficiency benchmark.

Table 4 and Figure 3 show that all series are multifractal, yet the degree and nature of inefficiency differ across assets. The two most efficient indices are ESR and CEI, whose spectrum peaks lie extremely close to the benchmark value of 0.5. The S&P Green Bond Index ranks fourth, with an inefficiency score of 0.0040. This is an important result because it places the green bond benchmark behind only the most stable broad ESG-style equity indices and ahead of more sector-sensitive sustainable assets.

The least efficient assets are the clean energy transition and natural-resources indices. The former likely reflects the valuation sensitivity of clean-energy firms to discount rates, policy incentives, and input-cost revisions. The latter combines commodity exposure, global-cycle sensitivity, and geopolitical dependence. That interpretation is reinforced by the fact that the natural-resources index also has the widest spectrum (2.4058), signalling the strongest multifractal heterogeneity in the sample.

The green bond benchmark is therefore best described as comparatively efficient rather than perfectly efficient. Its narrow spectrum and low volatility suggest a market segment with a more orderly scaling structure, but the estimated $\alpha_0$ remains different from 0.5. In other words, green bonds appear more resilient than most sustainable equity segments, yet they still embed nonlinear dependence and some degree of predictability. A plausible theoretical reading, which should be interpreted as a mechanism consistent with the evidence rather than directly identified by it, is that labelled debt markets benefit from more stable investor clienteles and clearer use-of-proceeds constraints, but remain exposed to climate-preference shocks and liquidity segmentation [14,15].

The fractal market hypothesis provides an economic channel through which these asset characteristics may be linked to the observed scaling properties. In this view, market stability depends on the coexistence of investors operating over different time horizons. When short-term, medium-term, and long-term participants remain active at the same time, liquidity can be supplied across scales and the dominant scaling exponent is more likely to remain close to the random-walk benchmark of 0.5 [24,25]. During crisis periods, this balance may weaken if short-horizon trading, forced deleveraging, or abrupt portfolio rebalancing becomes dominant. The resulting concentration of activity at particular horizons can fragment liquidity across scales and move the estimated scaling exponent away from 0.5. This mechanism is consistent with the cross-sectional pattern in Table 4. To the extent that green bond markets attract more stable institutional and buy-and-hold participation, their horizon structure may be less fragile than that of more speculative or sector-sensitive equity segments. By contrast, clean energy and natural-resources indices are more exposed to momentum-driven flows, policy repricing, commodity cycles, and speculative positioning. Their larger departures from the random-walk scaling benchmark may therefore be consistent with a more fragile horizon structure, rather than simply reflecting a higher level of conventional risk.

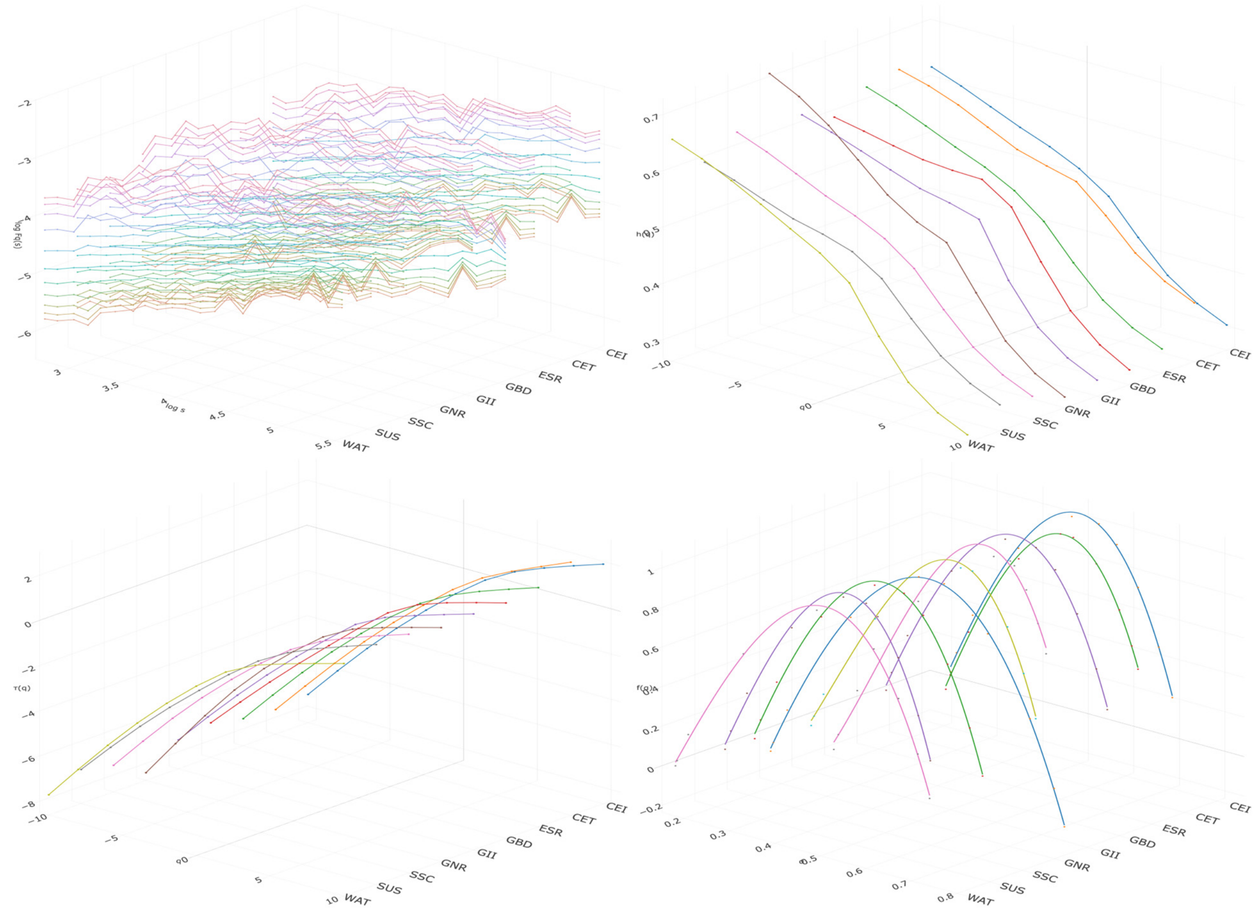


**Figure 3.** Full-sample MFDFA diagnostics: log–log fluctuation functions, generalized Hurst exponents, mass exponents, and fitted singularity spectra. In left-top panel, different colors represent the analyzed q-orders. In the rest panels, different colors distinguish the nine analyzed indices. In right-bottom panel, the points represent the estimated singularity spectra, while the continuous curves represent their polynomial fits.

## *4.3. Rolling Multifractal Evidence Across Crisis Regimes*

The dynamic results are easier to read when the local spectra, the time path of inefficiency, and the regime-specific averages are considered together. Figures 4–6 and Table 5 therefore provide a visual-to-summary sequence that links rolling geometry to the crisis segmentation adopted in the paper.

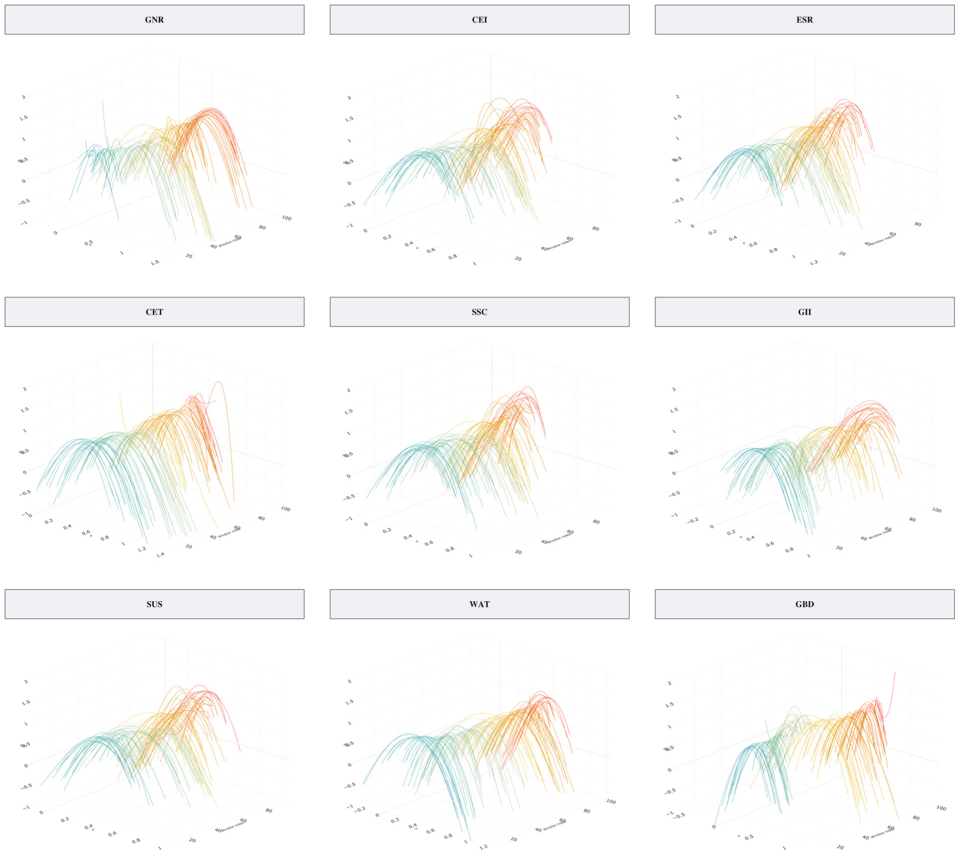


**Figure 4.** Rolling singularity spectra for all assets based on 500-day windows stepped by 21 trading days.


**Figure 5.** Rolling inefficiency trajectories across the nine assets. Shaded areas represent the assigned crisis regimes.

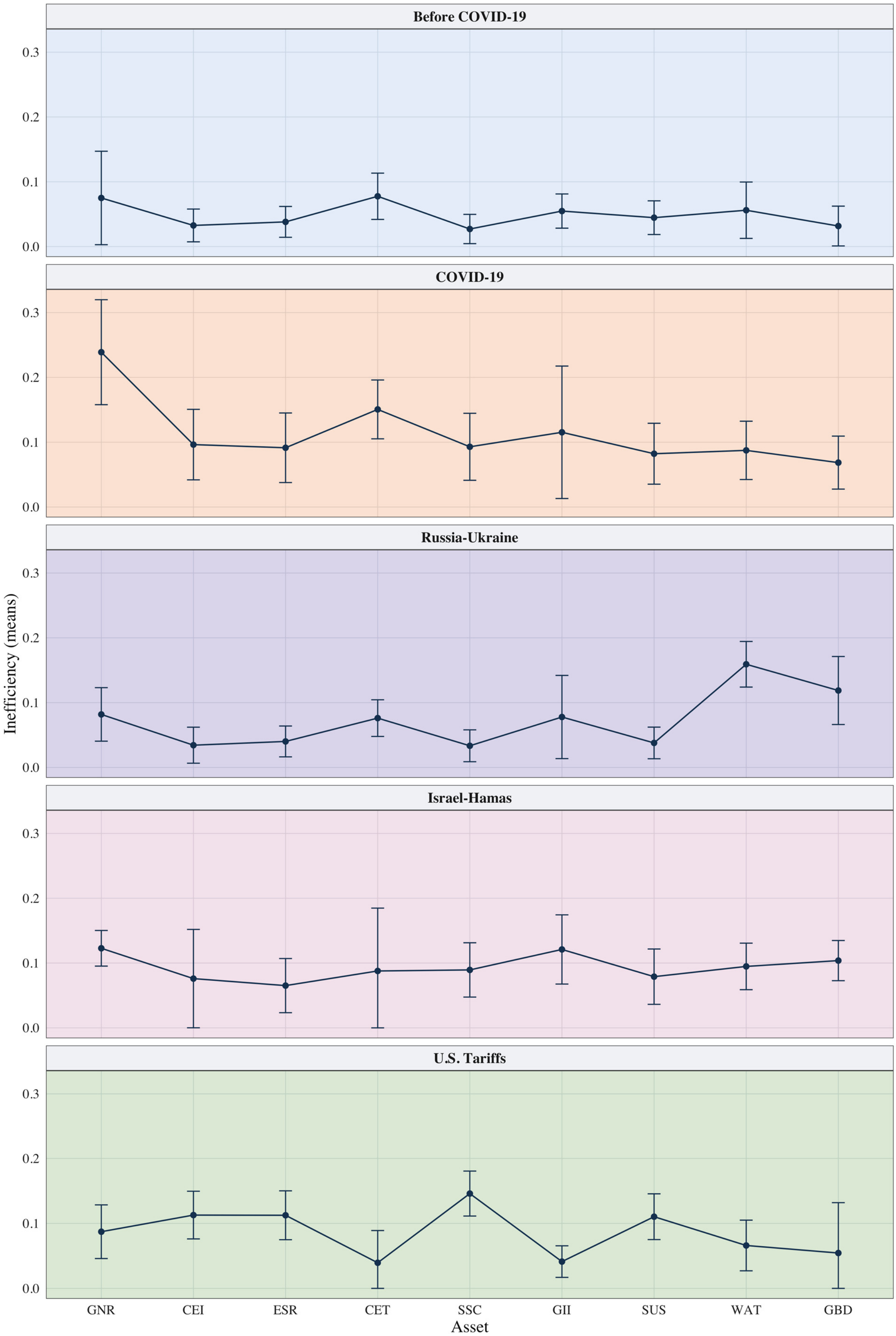


**Figure 6.** Regime-level averages and dispersion of rolling inefficiency.

**Table 5.** Regime-specific mean rolling inefficiency by asset.

| Code | Index | Before COVID-19 | COVID-19 | Russia–Ukraine | Israel–Hamas | U.S. Tariffs |
|---|---|---|---|---|---|---|
| GNR | S&P Global Natural Resources Index | 0.0750 (0.0721) | 0.2389 (0.0810) | 0.0818 (0.0413) | 0.1228 (0.0275) | 0.0872 (0.0413) |
| CEI | S&P 500 Carbon Efficient Index (USD) | 0.0326 (0.0253) | 0.0963 (0.0544) | 0.0343 (0.0278) | 0.0760 (0.0759) | 0.1128 (0.0367) |
| ESR | S&P 500 Environmental & Socially Responsible Index | 0.0381 (0.0238) | 0.0914 (0.0537) | 0.0401 (0.0238) | 0.0652 (0.0418) | 0.1125 (0.0376) |
| CET | S&P Global Clean Energy Transition Index (USD) | 0.0776 (0.0357) | 0.1506 (0.0454) | 0.0761 (0.0283) | 0.0878 (0.0970) | 0.0394 (0.0496) |
| SSC | S&P 500 Scored & Screened Index (USD) | 0.0271 (0.0226) | 0.0929 (0.0517) | 0.0334 (0.0246) | 0.0894 (0.0419) | 0.1459 (0.0346) |
| GII | S&P Global Infrastructure Index | 0.0548 (0.0264) | 0.1153 (0.1022) | 0.0778 (0.0642) | 0.1210 (0.0534) | 0.0412 (0.0243) |
| SUS | S&P 500 Sustainability Screened Index (USD) | 0.0446 (0.0260) | 0.0822 (0.0470) | 0.0378 (0.0244) | 0.0790 (0.0427) | 0.1103 (0.0352) |
| WAT | S&P Global Water Index | 0.0561 (0.0435) | 0.0874 (0.0450) | 0.1592 (0.0352) | 0.0948 (0.0359) | 0.0660 (0.0390) |
| GBD | S&P Green Bond Index | 0.0317 (0.0307) | 0.0685 (0.0409) | 0.1187 (0.0525) | 0.1038 (0.0310) | 0.0544 (0.0775) |

Entries are mean inefficiency values, with standard deviations in parentheses. Estimates are based on 500-day rolling windows stepped by 21 trading days.

The rolling evidence clearly rejects the idea of time-invariant efficiency. Average inefficiency rises from 0.0486 before COVID-19 to 0.1137 during the pandemic, an increase of 133.9%. Even after the pandemic, the market does not revert fully to the pre-crisis benchmark. The Russia–Ukraine, Israel–Hamas, and U.S. tariff regimes all remain above the initial level, although the magnitude of the effect differs across episodes.

Cross-sectional patterns are equally informative. The natural-resources index experiences the strongest jump during COVID-19, which is consistent with the commodity and macro-cycle channels that dominated that period. Water and green bonds display relatively stronger responses during the Russia–Ukraine regime, suggesting that geopolitical energy and inflation risks affected even the more defensive segments of the sustainable-finance universe. The U.S. tariff period, in turn, is especially relevant for CEI, ESR, SSC, and SUS, where the increase in inefficiency is pronounced despite the absence of a shock as globally synchronized as COVID-19.

This crisis heterogeneity is economically meaningful. COVID-19 acted as a common global stressor and produced a broad deterioration in efficiency, which is what one would expect when uncertainty, liquidity stress, and policy interventions simultaneously hit multiple asset classes. The later crises were narrower in origin, but they still affected market efficiency through more specific channels, such as energy repricing, geopolitical risk, trade policy, and the valuation of transition-sensitive sectors. That pattern is also compatible with the fractal-markets view that turbulent episodes are characterized by a temporary dominance of short horizons and reduced cross-horizon market balance [24,25].

Relative to the existing literature, these results extend the evidence in an important direction. Earlier studies showed that green bond efficiency worsened during COVID-19 and that multifractality remained sensitive to global factors [17,18]. The present evidence demonstrates that the crisis ranking itself is informative: systemic shocks remain the strongest disruptors of efficiency, but geopolitical and policy-driven regimes also matter and generate a more asset-specific pattern of inefficiency.

### 4.4. Regression Evidence

The regression evidence is presented as conditional, reduced-form evidence rather than as a causal event-study test. This framing is important because 500-day rolling windows can contain observations from more than one economic state. The estimates therefore answer a specific question: whether windows ending in crisis regimes display higher multifractal inefficiency than windows ending before COVID-19, after accounting for asset heterogeneity and, in robustness checks, local volatility and tail risk.

The regression section separates three layers of evidence. Table 6 reports OLS estimates with two-way clustered standard errors and a controlled specification that adds realized volatility, downside semideviation, and absolute tail risk. Table 7 preserves the quantile-regression evidence with bootstrap standard errors to show how crisis effects vary across the inefficiency distribution. Tables 8–10 summarize the robustness logic, the non-overlapping-window diagnostic, and the shuffled-series surrogate tests.

**Table 6.** Crisis-regime predictors of rolling inefficiency with dependence-robust inference.

| Model | Term | Estimate | Robust SE | *t*-Statistic | *p*-Value |
|---|---|---|---|---|---|
| Baseline, two-way clustered SE | Intercept | 0.0970 *** | 0.0049 | 19.7886 | 0.0000 |
| Baseline, two-way clustered SE | COVID-19 dummy | 0.0651 *** | 0.0146 | 4.4455 | 0.0000 |
| Baseline, two-way clustered SE | Russia–Ukraine dummy | 0.0246 * | 0.0140 | 1.7619 | 0.0784 |
| Baseline, two-way clustered SE | Israel–Hamas dummy | 0.0447 *** | 0.0081 | 5.5498 | 0.0000 |
| Baseline, two-way clustered SE | U.S. tariffs dummy | 0.0256 | 0.0157 | 1.6298 | 0.1035 |
| Controlled, two-way clustered SE | Intercept | 0.0618 *** | 0.0114 | 5.4011 | 0.0000 |
| Controlled, two-way clustered SE | COVID-19 dummy | 0.0151 | 0.0138 | 1.0994 | 0.2719 |
| Controlled, two-way clustered SE | Russia–Ukraine dummy | 0.0076 | 0.0172 | 0.4446 | 0.6567 |
| Controlled, two-way clustered SE | Israel–Hamas dummy | 0.0323 ** | 0.0135 | 2.3860 | 0.0172 |
| Controlled, two-way clustered SE | U.S. tariffs dummy | 0.0107 | 0.0125 | 0.8490 | 0.3961 |
| Controlled, two-way clustered SE | Realized volatility | 0.4025 | 1.1064 | 0.3638 | 0.7161 |
| Controlled, two-way clustered SE | Downside semideviation | 0.9416 | 1.1592 | 0.8123 | 0.4168 |
| Controlled, two-way clustered SE | Absolute tail risk p95 | −6.6137 * | 3.6495 | −1.8122 | 0.0703 |

The baseline model includes crisis-regime dummies and asset fixed effects. The controlled model additionally includes realized volatility, downside semideviation, and the 95th percentile of absolute returns computed inside each rolling window. Standard errors are clustered by asset and rolling-window identifier. Statistical significance: *** $p < 0.01$, ** $p < 0.05$, * $p < 0.10$.

Table 6 shows that the signs of all crisis coefficients remain positive when two-way clustered standard errors are used. In the baseline specification, COVID-19 and Israel–Hamas remain strongly significant, Russia–Ukraine remains marginally significant, and the U.S. tariff coefficient remains positive but is no longer significant at conventional levels. After adding volatility and tail-risk controls, the crisis coefficients remain positive, but their magnitudes decline and only the Israel–Hamas coefficient remains statistically significant. This result has a substantive economic implication beyond the adjustment of standard errors. The attenuation of the crisis coefficients after conditioning on volatility and tail risk suggests that the association between crisis-labelled windows and multifractal inefficiency operates to a considerable extent through changes in the distributional properties of returns. Put differently, the evidence does not strongly support a separate crisis-regime channel that remains independent of volatility and tail behaviour. The COVID-19 coefficient, which is the largest and most significant in the baseline specification, falls sharply and loses significance once these distributional conditions are absorbed. This pattern suggests that the pandemic-related increase in multifractal inefficiency was closely connected to the extreme return environment generated by liquidity compression, large price adjustments, and unprecedented policy interventions, rather than to a clearly separable disruption in the informational structure of prices. The Israel–Hamas coefficient is the only crisis coefficient that remains statistically significant in the controlled specification, which may point to a geopolitical uncertainty channel that affects price formation without generating proportional changes in the included volatility and tail-risk measures. However, this interpretation should remain cautious because the regime contains a relatively small number of rolling-window endpoints. The broader implication is that within-window distributional conditions are central to understanding time-varying multifractal efficiency in sustainable-finance markets, and crisis labels should be read as regime descriptors rather than as independently identified causal forces.

**Table 7.** Quantile-regression crisis effects with bootstrap standard errors.

| Quantile | Term | Estimate | Bootstrap SE | *t*-Statistic | *p*-Value |
|---|---|---|---|---|---|
| 0.10 | COVID-19 dummy | 0.0111 ** | 0.0046 | 2.4367 | 0.0150 |
| 0.10 | Russia–Ukraine dummy | 0.0082 *** | 0.0027 | 3.0478 | 0.0024 |
| 0.10 | Israel–Hamas dummy | 0.0227 *** | 0.0045 | 5.0960 | 0.0000 |
| 0.10 | U.S. tariffs dummy | 0.0060 | 0.0045 | 1.3382 | 0.1812 |
| 0.25 | COVID-19 dummy | 0.0408 *** | 0.0072 | 5.6745 | 0.0000 |
| 0.25 | Russia–Ukraine dummy | 0.0093 ** | 0.0047 | 1.9841 | 0.0476 |
| 0.25 | Israel–Hamas dummy | 0.0331 *** | 0.0049 | 6.7337 | 0.0000 |
| 0.25 | U.S. tariffs dummy | 0.0060 | 0.0084 | 0.7150 | 0.4748 |
| 0.50 | COVID-19 dummy | 0.0648 *** | 0.0069 | 9.4515 | 0.0000 |
| 0.50 | Russia–Ukraine dummy | 0.0205 *** | 0.0062 | 3.3065 | 0.0010 |
| 0.50 | Israel–Hamas dummy | 0.0446 *** | 0.0074 | 6.0502 | 0.0000 |
| 0.50 | U.S. tariffs dummy | 0.0201 | 0.0167 | 1.2011 | 0.2300 |
| 0.75 | COVID-19 dummy | 0.0868 *** | 0.0064 | 13.5917 | 0.0000 |
| 0.75 | Russia–Ukraine dummy | 0.0254 *** | 0.0075 | 3.3689 | 0.0008 |
| 0.75 | Israel–Hamas dummy | 0.0453 *** | 0.0077 | 5.8781 | 0.0000 |
| 0.75 | U.S. tariffs dummy | 0.0490 *** | 0.0140 | 3.4914 | 0.0005 |
| 0.90 | COVID-19 dummy | 0.0956 *** | 0.0076 | 12.6501 | 0.0000 |
| 0.90 | Russia–Ukraine dummy | 0.0452 ** | 0.0193 | 2.3365 | 0.0197 |
| 0.90 | Israel–Hamas dummy | 0.0594 *** | 0.0143 | 4.1484 | 0.0000 |
| 0.90 | U.S. tariffs dummy | 0.0807 *** | 0.0170 | 4.7394 | 0.0000 |

Entries report crisis-regime coefficients from quantile regressions with asset fixed effects. Standard errors are bootstrap estimates with 200 replications. Statistical significance: *** $p < 0.01$, ** $p < 0.05$.

A methodological caution should nevertheless be noted for this controlled specification. The within-window controls, namely realized volatility, downside semideviation, and the 95th percentile of absolute returns, are computed from the same return series used to estimate the MFDFA statistics. Because the singularity spectrum and its peak are themselves functions of the scaling and distributional properties of returns, the controls and the dependent variable share a common statistical basis. The attenuation of crisis coefficients may therefore reflect, at least in part, this mechanical overlap rather than a clean decomposition of crisis effects into distributional and non-distributional channels. External variables that describe the crisis environment without being computed from the same return windows, such as the VIX, credit spreads, funding-liquidity measures, policy-uncertainty indices, or direct market-liquidity proxies, would provide a stronger identification strategy. These variables are not included in the present dataset, and their incorporation remains an important direction for future research.

**Table 8.** Robustness and sensitivity checks.

| Check | Implementation | Result |
|---|---|---|
| Two-way clustered inference | OLS re-estimated with standard errors clustered by asset and rolling-window identifier. | The signs of all crisis coefficients remain positive under dependence-robust inference. |
| Bootstrap quantile inference | Quantile regressions re-estimated with bootstrap standard errors for the crisis-regime coefficients. | The upper-tail amplification of COVID-19 and Israel–Hamas effects remains visible under bootstrap inference. |
| Distributional controls | OLS augmented with realized volatility, downside semideviation, and the 95th percentile of absolute returns computed inside each rolling window. | Crisis coefficients remain positive after controlling for window-level volatility and tail risk; magnitudes are interpreted as conditional reduced-form effects. |
| Non-overlapping windows | Baseline OLS re-estimated on a greedily selected set of windows with no date overlap within each asset. | The non-overlapping check preserves the positive direction of the main crisis effects, although precision is lower due to the smaller sample. |
| Regime assignment | The ending-date assignment is retained and explicitly described as a classification rule, not a causal event-study design. | Claims were moderated from causal language to regime-conditional association. |
| Source of multifractality | Shuffled-series surrogate tests preserve the unconditional return distribution while destroying temporal ordering. | Several assets retain larger original spectrum widths than their shuffled counterparts, while others are mainly distribution-driven; the evidence therefore points to mixed sources of multifractality. |

The checks are designed to address overlapping-window dependence, distributional confounding, regime assignment, and the interpretation of multifractal inefficiency. The non-overlapping-window check is diagnostic because it contains only 45 observations.

**Table 9.** Non-overlapping-window sensitivity check.

| Term | Estimate | HC1 SE | *t*-Statistic | *p*-Value |
|---|---|---|---|---|
| Intercept | 0.0958 *** | 0.0322 | 2.9782 | 0.0054 |
| COVID-19 dummy | 0.0216 | 0.0181 | 1.1949 | 0.2406 |
| Russia–Ukraine dummy | 0.0316 * | 0.0167 | 1.8910 | 0.0674 |
| U.S. tariffs dummy | 0.0496 * | 0.0288 | 1.7191 | 0.0950 |

Windows were selected greedily so that no two windows overlap within each asset. The smaller sample reduces precision, but the positive direction of the main crisis coefficients is preserved where the dummy is estimable. * and *** indicate statistical significance at the 10% and 1% levels, respectively.

**Table 10.** Shuffled-series surrogate test for sources of multifractality.

| Asset | Original Width | Mean Shuffled Width | Shuffled 2.5% | Shuffled 97.5% | Dependence Share | Replications |
|---|---|---|---|---|---|---|
| CEI | 0.4870 | 0.4979 | 0.3244 | 0.6716 | 0.0000 | 200 |
| CET | 0.4222 | 0.3781 | 0.1944 | 0.5749 | 0.1044 | 200 |
| ESR | 0.4857 | 0.4882 | 0.2773 | 0.6845 | 0.0000 | 200 |
| GBD | 0.4664 | 0.3209 | 0.1485 | 0.4966 | 0.3120 | 200 |
| GII | 0.4933 | 0.5551 | 0.3451 | 0.7427 | 0.0000 | 200 |
| GNR | 0.6452 | 0.4294 | 0.2405 | 0.6307 | 0.3344 | 200 |
| SSC | 0.5006 | 0.4815 | 0.2653 | 0.6824 | 0.0381 | 200 |
| SUS | 0.4508 | 0.4768 | 0.2560 | 0.6554 | 0.0000 | 200 |
| WAT | 0.5583 | 0.4596 | 0.2496 | 0.6404 | 0.1768 | 200 |

The shuffled test preserves the unconditional return distribution but destroys temporal ordering. A positive dependence share indicates that the original raw spectrum width exceeds the mean shuffled width, suggesting a temporal-dependence contribution beyond distributional shape. The surrogate exercise uses 200 shuffled replications per asset; the 2.5% and 97.5% columns report the empirical interval of the shuffled-width distribution. Phase-randomized procedures remain a useful extension.

The bootstrap quantile regressions add a distributional insight that is robust to a more cautious inferential treatment. The COVID-19 coefficient increases from 0.0111 at the 10th percentile to 0.0956 at the 90th percentile, indicating that the pandemic disproportionately amplified already inefficient states. The Israel–Hamas coefficient remains positive and significant across all reported quantiles, and the U.S. tariff coefficient becomes significant in the upper tail. This pattern supports the view that policy-driven shocks may be mild in low-inefficiency windows but materially destabilizing when markets are already fragile (Figure 7).

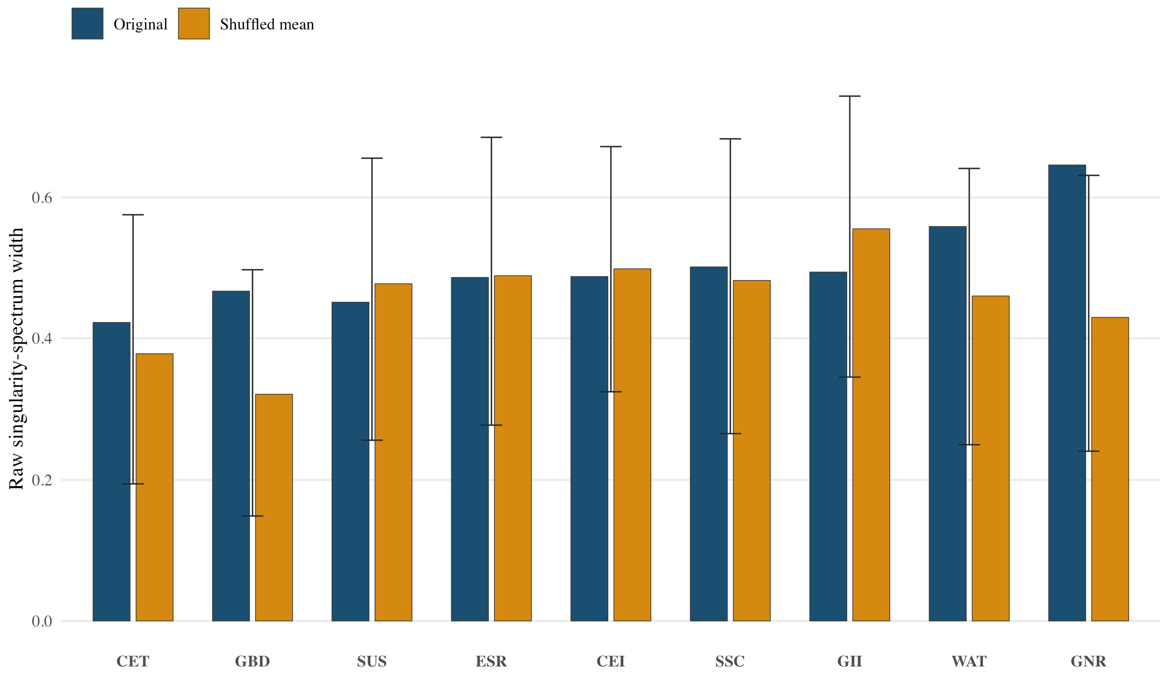


**Figure 7.** Original and shuffled-series raw singularity-spectrum widths. Shuffling preserves the unconditional return distribution while removing temporal ordering; larger original widths therefore indicate a stronger temporal-dependence contribution. Error bars show the empirical 2.5% to 97.5% interval of the 200 shuffled replications.

These additional checks lead to a more conservative interpretation of the evidence. The main finding is not that crisis dummies fully identify informational inefficiency independently of all risk conditions. The stronger claim is that crisis-labelled windows exhibit higher multifractal inefficiency and that this pattern remains directionally stable under dependence-robust inference, risk controls, bootstrap quantile inference, and a non-overlapping-window diagnostic. The shuffled-series tests further show mixed sources of multifractality: GNR, GBD, WAT, and CET retain positive dependence shares, whereas CEI, GII, and SUS are closer to distribution-driven multifractality. Because the surrogate exercise uses 200 shuffled replications per asset, the shuffled mean is less sensitive to simulation noise, while the results remain best interpreted as a robustness diagnostic rather than as a fully calibrated resampling test. This interpretation also aligns the paper with semi-strong efficiency evidence showing that public information shocks can generate persistent abnormal-return dynamics [32] and with distributional work showing that skewness and heavy tails can materially affect inference in financial returns [33].

### *4.5. Interpretation and Broader Implications*

Taken together, the evidence supports a regime-dependent and adaptive reading of market efficiency. The Adaptive Markets Hypothesis implies that efficiency is not a permanent market characteristic but the outcome of a changing interaction between information, incentives, market structure, and investor learning [13]. The sustainable-finance universe examined here behaves in exactly that way. At the same time, the fractal markets perspective emphasizes that stability depends on the coexistence of heterogeneous investment horizons and liquidity across scales [24,25]. Efficiency improves in some periods, deteriorates in others, and reacts differently depending on whether the shock is systemic, geopolitical, or policy-related.

The green bond benchmark emerges as relatively resilient, but the analysis avoids attributing that resilience to unobserved mechanisms as if they had been directly tested. Stable investor clienteles, use-of-proceeds constraints, and debt-market liquidity are plausible channels, but the dataset does not include fund flows, bid–ask spreads, issuance characteristics, or direct clientele measures. The discussion therefore treats these channels as theoretically consistent explanations rather than as independently identified empirical mechanisms. This distinction also matters for portfolio interpretation: time-series multifractal efficiency is related to, but not the same as, portfolio efficiency or optimal allocation under changing risk capacity [31,34].

For portfolio management, the results imply that sustainable assets should not be treated as a homogeneous block. Broad ESG-style equity benchmarks such as CEI and ESR display stronger full-sample efficiency, whereas sectoral indices tied to energy transition, natural resources, or infrastructure are more exposed to nonlinear persistence. For researchers, the main implication is that sustainable-finance efficiency is better understood through dynamic and crisis-comparative methods than through static full-sample averages alone.

## 5. Conclusions

This paper examined the dynamic multifractal efficiency of green bonds and sustainable equity indices with a common MF-DFA framework applied to daily index-level data from 2016 to 2025. The evidence shows that the S&P Green Bond Index is relatively close to the random-walk scaling benchmark and is clearly less volatile than the sustainable equity indices, but the paper does not present this result as proof of general portfolio superiority or crisis immunity. It is instead interpreted as evidence of comparatively lower time-series persistence in the dominant scaling exponent.

The broader implication is that sustainable-finance efficiency is nonlinear, state dependent, and partly entangled with volatility and tail conditions. Crisis-labelled windows are associated with higher rolling inefficiency, but the robustness checks show that statistical strength varies once dependence and distributional controls are introduced. Future research should extend the analysis with direct liquidity, flow, and sector-composition variables; external uncertainty indices; shuffled and phase-randomized surrogate tests; and alternative MFDFA parameterizations. These extensions would help separate dependence-driven multifractality from distribution-driven multifractality and further clarify the economic sources of efficiency loss in sustainable finance.

**Author Contributions:** F.H.A.d.A.: Conceptualization, data curation, formal analysis, software, visualization, writing—original draft, funding acquisition. M.K.: Conceptualization, methodology, validation, supervision, writing—review and editing. P.M.: Methodology, validation, writing—review and editing. All authors have read and agreed to the published version of the manuscript.

**Funding:** This work was supported by the Conselho Nacional de Desenvolvimento Cientifico e Tecnologico (CNPq), Brazil, through a Research Productivity Grant awarded to Fernando Henrique Antunes de Araujo. This article was supported by Ministry of Science, Technological Development and Innovation of the Republic of Serbia under Contract No. 451-03-47/2023-01/200005. The funder had no role in study design, data collection, analysis, interpretation, writing of the report, or the decision to submit the article for publication.

**Data Availability Statement:** The data supporting the findings of this study are available from the corresponding author upon reasonable request.

**Acknowledgments:** The author Fernando H. A. Araujo thanks the Sacred Heart of Jesus and the Immaculate Heart of Mary.

**Conflicts of Interest:** The authors declare no conflicts of interest.

## References

1. Reboredo, J.C. Green bond and financial markets: Co-movement, diversification and price spillover effects. *Energy Econ.* **2018**, *74*, 38–50. [CrossRef]
2. Broadstock, D.C.; Chatziantoniou, I.; Gabauer, D. Minimum Connectedness Portfolios and the Market for Green Bonds: Advocating Socially Responsible Investment (SRI) Activity. In *Applications in Energy Finance*; Floros, C., Chatziantoniou, I., Eds.; Palgrave Macmillan: Cham, Switzerland, 2022; pp. 223–251. [CrossRef]
3. Flammer, C. Corporate green bonds. *J. Financ. Econ.* **2021**, *142*, 499–516. [CrossRef]
4. International Capital Market Association. *Green Bond Principles: Voluntary Process Guidelines for Issuing Green Bonds*; ICMA: Zurich, Switzerland, 2021. Available online: https://www.icmagroup.org/assets/documents/Sustainable-finance/2021-updates/Green-Bond-Principles-June-2021-140621.pdf (accessed on 21 May 2026).
5. Baur, D.G.; Lucey, B.M. Is gold a hedge or a safe haven? An analysis of stocks, bonds and gold. *Financ. Rev.* **2010**, *45*, 217–229. [CrossRef]
6. Guo, D.; Zhou, P. Green bonds as hedging assets before and after COVID: A comparative study between the US and China. *Energy Econ.* **2021**, *104*, 105696. [CrossRef]
7. Chopra, M.; Mehta, C. Going green: Do green bonds act as a hedge and safe haven for stock sector risk? *Financ. Res. Lett.* **2023**, *51*, 103357. [CrossRef]
8. Arif, M.; Naeem, M.A.; Farid, S.; Nepal, R.; Jamasb, T. Diversifier or more? Hedge and safe haven properties of green bonds during COVID-19. *Energy Policy* **2022**, *168*, 113102. [CrossRef] [PubMed]
9. Reboredo, J.C.; Ugolini, A. Price connectedness between green bond and financial markets. *Econ. Model.* **2020**, *88*, 25–38. [CrossRef]
10. Karim, S.; Lucey, B.M.; Naeem, M.A.; Yarovaya, L. Extreme risk dependence between green bonds and financial markets. *Eur. Financ. Manag.* **2024**, *30*, 935–960. [CrossRef]
11. Fama, E.F. Efficient capital markets: A review of theory and empirical work. *J. Financ.* **1970**, *25*, 383–417. [CrossRef]
12. Grossman, S.J.; Stiglitz, J.E. On the impossibility of informationally efficient markets. *Am. Econ. Rev.* **1980**, *70*, 393–408. Available online: https://www.jstor.org/stable/1805228 (accessed on 21 May 2026).
13. Lo, A.W. The Adaptive Markets Hypothesis: Market efficiency from an evolutionary perspective. *J. Portf. Manag.* **2004**, *30*, 15–29. [CrossRef]
14. Pástor, L'.; Stambaugh, R.F.; Taylor, L.A. Sustainable investing in equilibrium. *J. Financ. Econ.* **2021**, *142*, 550–571. [CrossRef]
15. Bongaerts, D.; Schoenmaker, D. Liquidity and clientele effects in green debt markets. *J. Corp. Financ.* **2024**, *86*, 102582. [CrossRef]
16. Calvet, L.E.; Fisher, A.J. Multifractality in asset returns: Theory and evidence. *Rev. Econ. Stat.* **2002**, *84*, 381–406. [CrossRef]
17. Naeem, M.A.; Farid, S.; Ferrer, R.; Shahzad, S.J.H. Comparative efficiency of green and conventional bonds pre- and during COVID-19: An asymmetric multifractal detrended fluctuation analysis. *Energy Policy* **2021**, *153*, 112285. [CrossRef]
18. Vo, X.V.; Kang, S.H. Upside-downside multifractality and efficiency of green bonds: The roles of global factors and COVID-19. *Financ. Res. Lett.* **2021**, *43*, 101995. [CrossRef]
19. Zhuang, X.; Wei, D. Asymmetric multifractality, comparative efficiency analysis of green finance markets: A dynamic study by index-based model. *Phys. A* **2022**, *604*, 127949. [CrossRef]
20. Kojić, M.; Mitić, P.; Schluter, S.; Rakić, S. Complex non-linear relationship between conventional and green bonds: Insights amidst COVID-19 and the RU-UA conflict. *J. Behav. Exp. Financ.* **2024**, *43*, 100966. [CrossRef]
21. Lalwani, V. Climate risks, corporate bonds, and economic uncertainty. *Econ. Lett.* **2024**, *244*, 111984. [CrossRef]
22. Mensi, W.; Lee, Y.-J.; Al-Yahyaee, K.H.; Sensoy, A.; Yoon, S.-M. Intraday downward/upward multifractality and long memory in Bitcoin and Ethereum markets: An asymmetric multifractal detrended fluctuation analysis. *Financ. Res. Lett.* **2019**, *31*, 19–25. [CrossRef]
23. Urquhart, A. The inefficiency of Bitcoin. *Econ. Lett.* **2016**, *148*, 80–82. [CrossRef]
24. Kristoufek, L. Fractal markets hypothesis and the global financial crisis: Wavelet power evidence. *Sci. Rep.* **2013**, *3*, 2857. [CrossRef]
25. Lahmiri, S.; Bekiros, S.; Bezzina, F. Evidence of the fractal market hypothesis in European industry sectors with the use of bootstrapped wavelet leaders singularity spectrum analysis. *Chaos Solitons Fractals* **2022**, *165*, 112813. [CrossRef]

26. Kantelhardt, J.W.; Zschiegner, S.A.; Koscielny-Bunde, E.; Havlin, S.; Bunde, A.; Stanley, H.E. Multifractal detrended fluctuation analysis of nonstationary time series. *Phys. A* **2002**, *316*, 87–114. [CrossRef]
27. Fernandes, L.H.S.; de Araujo, F.H.A.; Tabak, B.M. Insights from the (in)efficiency of Chinese sectoral indices during COVID-19. *Phys. A* **2021**, *578*, 126063. [CrossRef]
28. de Araujo, F.H.A.; Fernandes, L.H.S.; Tabak, B.M. Effects of COVID-19 on Chinese sectoral indices: A multifractal analysis. *Fractals* **2021**, *29*, 2150198. [CrossRef]
29. Fernandes, L.H.S.; Fernandes, J.P.V.; Silva, J.W.L.; Paiva, R.O.A.; Pinto, I.M.B.S.; de Araujo, F.H.A. The (in)efficiency of USA education group stocks: Before, during and after COVID-19. *Fractals* **2024**, *32*, 2450047. [CrossRef]
30. Papla, D.; Siedlecki, R. Entropy as a tool for the analysis of stock market efficiency during periods of crisis. *Entropy* **2024**, *26*, 1079. [CrossRef]
31. Agrrawal, P. The Gibbons, Ross, and Shanken test for portfolio efficiency: A note based on its trigonometric properties. *Mathematics* **2023**, *11*, 2198. [CrossRef]
32. Agrrawal, P.; Agarwal, R. A longer-term evaluation of information releases by influential market agents and the semi-strong market efficiency. *J. Behav. Financ.* **2025**, *26*, 20–45. [CrossRef]
33. Yuan, J.; Zhang, Z. Construction and applications of a composite model based on skew-normal and skew-t distributions. *Econometrics* **2025**, *13*, 48. [CrossRef]
34. Waggle, D.; Agrrawal, P. Guaranteed income and optimal retirement glide paths. *J. Financ. Plan.* **2024**, *37*, 74–94.